rotation and a stable, inhomogeneous surface composition for the B star to explain the behaviour of the He line[4,13].

Bolton's[14] upper limit to the radial velocity variation of σ Ori E implies that any companion must have a mass $\lesssim 0.1 M_\odot$ for inclinations > 45°. Thus the secondary would be an M dwarf or a collapsed object. The latter alternative would be in agreement with the above model, as well as providing a ready explanation for the helium enhancement (or hydrogen deficiency) at the surface of σ Ori E in terms of a prior episode of mass transfer from an originally more massive companion. Since σ Ori E is located in a Trapezium-like system containing a 09.5-V component[2], the mass of the original primary in the mass-transfer binary picture would have been $\gtrsim 20 M_\odot$.

If this model is correct, high-frequency optical monitoring of σ Ori E might provide additional information; only one such study has been made at CTIO, before the development of the present working picture, and hence at a rather low sampling frequency. Beginning at 1974 December 6.084 UT, σ Ori E was monitored at Hα for 6 h with the 3-channel photometer at the 0.9-m telescope. A 20/80% neutral beamsplitter, 2 FW 130 (S20) photocells, and KPNO filters 210 ($\Delta\lambda$ = 159 Å) and 71 ($\Delta\lambda$ = 54 Å) were used for 2-s integrations. A total of 8,192 integrations was processed with power spectral techniques[15]; no peak > 0.0013 mag was found in the period range $4.0 < P <$ 1,640 s for the sampled phases.

While this paper was in preparation, an alternative but related interpretation of the light curves of σ Ori E occurred to one of us (N.R.W.) after reading the new results on Algol[16]. The alternative model follows from interpreting the two minima in σ Ori E as components of a single 'W-shaped' eclipse; indeed, the resulting ingress–egress symmetries strongly support the correctness of such an interpretation. In this case one is led to consider two ultraviolet-bright spots, most probably located at the equilateral Lagrangian points of the binary system, with the leading spot somewhat the brighter. 'Mid-eclipse' occurs at $\varphi \simeq 0.83$, with both Lagrangian points visible. The mass ratio condition for the existence of stable, equilateral Lagrangian points implies an upper limit to the secondary mass of the same order as that resulting from the radial velocity observations. If a plausible model with $\mathcal{M}_1 = 8 M_\odot$, $\mathcal{M}_2 = 0.1 M_\odot$, and centre-to-centre separation of two primary radii is assumed, the resulting geometry is strikingly simple, and many features of the light and colour curves are explained in a straightforward manner.

The implications of this model of σ Ori E for current theories of stellar evolution in massive binaries are sufficiently significant to justify extensive further observations. Most critically needed are high-accuracy radial velocities throughout the full 1.19 d cycle, preferably with simultaneous photoelectric monitoring. In addition, polarimetric, X-ray and radio observations of both moderate- and high-time resolution may provide key information for the evaluation of the proposed working model.

J.E.H. thanks Dr John Irwin for relinquishing a crucial night of telescope time; Sr. Guido Garay for programming assistance and the Yale University Observatory for their hospitality while this paper was being written. The Cerro Tololo Observatory is operated by the Association of Universities for Research in Astronomy, Inc., under contract with the NSF.

JAMES E. HESSER
NOLAN R. WALBORN
PATRICIO UGARTE P.

Cerro Tololo Inter-American Observatory, La Serena, Chile

Received February 19; accepted May 7, 1976.

1 Berger, J., *C. Inst. Astrophys Paris*, A217 (1956).
2 Greenstein, J. L., and Wallerstein, G., *Astrophys. J.*, **127**, 237 (1958).
3 Walborn, N. R., *Astrophys. J. Lett.*, **191**, L95 (1974).
4 Walborn N. R., and Hesser, J. E., *Astrophys. J. Lett.*, **205**, L87 (1976).
5 Crawford, D. L., and Barnes, J. V., *Astr. J.*, **75**, 978 (1970).
6 Crawford, D. L., and Mander, J. V., *Astr. J.*, **71**, 114 (1966).
7 Hesser, J. E., and Ugarte P., *IAU Circ.*, No. 2911 (1976).
8 Kraft, R. P., *Astrophys. J.*, **135**, 408 (1962).
9 Krzeminski, W., *Astrophys. J.*, **142**, 1051 (1965).
10 Smak, J., *Acta Astr.*, **19**, 287 (1969).
11 Warner B., and Nather, E., *Mon. Not. R. astr. Soc.*, **152**, 219 (1971).
12 Lin, D. N. C., *Mon. Not. R. astr. Soc.*, **170**, 379 (1975).
13 Thomsen, B., *Astr. Astrophys.*, **35**, 479, (1974).
14 Bolton, C. T., *Astrophys. J. Lett.*, **192**, L7 (1974).
15 Hesser, J. E., and Lasker, B. M., in *Proc. of IAU Colloq.*, **15**; *Veröff. der Remeis-Sternwarte Bamberg*, **9**, 1960 (1971).
16 Guinan, E. F., McCook, G. P., Bachmann, P. J., and Bistline, W. G., *Astr. J.*, **81**, 57 (1976).

Evidence for a radioactive decay hypothesis for supernova luminosity

VAN HISE[1] has observed that the light curve for the Type I supernova 1937c is well represented by a sum of two exponentials with half lives which are ~0.75 the half lives of ^{56}Ni and ^{56}Co in the β-decay chain $^{56}\text{Ni} \rightarrow ^{56}\text{Co} \rightarrow ^{56}\text{Fe}$. Colgate and McKee[2] had previously suggested this chain as a source of supernova luminosity, but the hypothesis was not widely accepted because of the variability of the decay rates of supernova light curves and because the interstellar medium would be overabundant in heavy elements. This letter presents observational evidence supporting a model of Leventhal and McCall[3] which overcomes these difficulties.

According to this model, a Type I supernova produces a white dwarf containing $\sim 0.2 M_\odot$ of ^{56}Ni. At terrestrial densities the decays of ^{56}Ni and ^{56}Co occur by capture of an inner shell electron 100 and 80% of the time, respectively, but in the interior of a white dwarf, the bare nuclei move through a Fermi sea of electrons, and the higher electron densities thus encountered would produce an enhancement of the decay rates. The supernova luminosity is given by

$$L(t) = A_1 \exp(-t/T_1) + A_2 \exp(-t/T_2) \qquad (1)$$

where T_1 and T_2 are the half lives of the steep, earlier and the flat, later portions of the light curve, and A_1 and A_2 are parameters whose values depend on the initial amount of ^{56}Ni, the

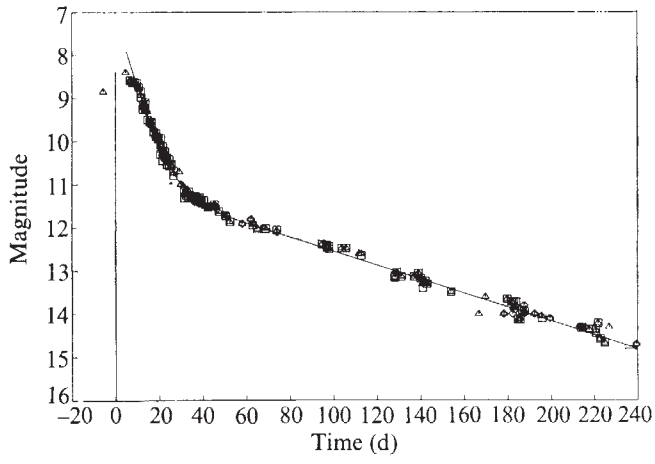

Fig. 1 Sum of exponentials fit to the light curve of SN1937c. The vertical line at $t = 0$ represents the estimate m_0 of peak apparent magnitude. □, Baade and Zwicky[9]; △, Parenago[10]; ◇, Deutsch[11]. For the values of the parameters of the fit see Table 1.

energy releases per decay of ^{56}Ni and ^{56}Co, and the values of T_1 and T_2. If the model is correct, T_1 should not exceed the terrestrial half life of ^{56}Ni (8.8 d), T_2 should not exceed that of ^{56}Co (112 d), and the two should be related approximately by

$$\frac{T_1}{8.8} = \frac{T_2}{112}; \; T_2 = 12.7\, T_1 \qquad (2)$$

More precisely, according to Leventhal and McCall[3], at

Table 1 Results of the sum of exponentials fits

Supernova	Galaxy	$\frac{A_1}{L_0} \pm \sigma\frac{A_1}{L_0}$	$T_1 \pm \sigma(T_1)$	$\frac{A_2}{L_0} \pm \sigma\frac{A_2}{L_0}$	$T_2 \pm \sigma(T_2)$
1937c	IC4182	3.18±0.13	6.47±0.16	0.0980±0.0088	67.2±6.8
1937d	NGC1003	1.36±0.11	9.26±1.09	0.0708±0.0471	102.1±92.4
1939a	NGC4636	3.07±1.45	4.12±1.34	0.159±0.073	59.3±33.7
1954a	NGC4214	1.52±0.14	4.14±0.32	0.142±0.014	55.6±5.4
1954b	NGC5668	2.19±0.56	5.70±1.16	0.0964±0.0513	75.9±54.9
1956a	NGC3992	11.9±6.5	4.59±0.70	0.0896±0.0302	87.7±38.4
1957a	NGC2841	1.82±0.25	4.55±0.43	0.130±0.021	47.4±8.4
1961p	Anon.	1.64±0.07	10.3±0.7	0.0979±0.0259	112.3±40.5
1962j	NGC6835	3.14±1.12	7.48±1.34	0.111±0.048	114.8±81.4
1962l	NGC1073	3.39±0.78	5.21±0.77	0.181±0.064	68.1±34.6
1963p	NGC1084	5.44±1.19	4.96±0.44	0.0684±0.0217	61.2±20.5
1964l	NGC3938	2.65±0.49	5.96±0.46	0.0671±0.0081	120.4±22.9
1966j	NGC3198	4.44±2.18	7.11±1.01	0.0766±0.0108	112.3±22.4
1966n	Anon.	1.34±0.10	8.38±1.36	0.0917±0.0384	85.4±44.7
1967c	NGC3389	2.17±0.19	8.17±1.00	0.129±0.101	47.9±30.4

high matter densities the ^{56}Ni and ^{56}Co decay rates (d^{-1}) are given by

$$R_{Ni}=\frac{1}{8.8}\left(\frac{\bar{\rho}_{av}}{9.7\times10^{28}}\right)(1+0.61\times10^{10}\,\bar{\rho}_{av}^{-1/3})$$

$$R_{Co}=\frac{1}{558}+\frac{1}{139.4}\left(\frac{\bar{\rho}_{av}}{8.6\times10^{28}}\right)(1+0.60\times10^{10}\,\bar{\rho}_{av}^{-1/3})$$

where $\bar{\rho}_{av}$ is the electron density (cm^{-3}), 8.8 and 112 d are the terrestrial 1/e lives of ^{56}Ni and ^{56}Co, 9.7×10^{28} and 8.6×10^{28} cm^{-3} are the electron densities at Ni and Co nuclei in the terrestrial environment, and 1/558 d^{-1} represents the fraction (20% on Earth) of Co decays which involve positron emission. It is assumed here that the positron emission rate is unaffected by high densities. At low densities, electron binding occurs, so the effective decay rates can be calculated by the interpolation equations

$$T_1=\left[\left(\frac{1}{8.8}\right)^2+R_{Ni}^{\,2}\right]^{-1/2}$$

$$T_2=\left[\left(\frac{1}{112}\right)^2+R_{Co}^{\,2}\right]^{-1/2}$$

which define a curve well approximated by the straight line, equation (2).

Rust[4] has recently collected 37 Type I light curves from the literature and used techniques developed by Pskovskii[5,6] to reduce them to a common photometric system (the m_{pg} system). Fifteen of the curves were complete enough to give reasonable fits using a sum of two exponentials. The others did not extend far enough to define the more slowly decaying exponential.

The light curves consisted of measurements of apparent magnitude $m(t)$ versus time. Apparent magnitude is related to luminosity by

$$\frac{L(t)}{L_0}=10^{-0.4[m(t)-m_0]} \qquad (3)$$

where L_0 and m_0 are the luminosity and apparent magnitude at maximum brightness. Taking the moment of peak brightness as the zero-point of time and combining equations (1) and (3) gives

$$10^{-0.4[m(t)-m_0]}=\frac{A_1}{L_0}\exp(-t/T_1)+\frac{A_2}{L_0}\exp(-t/T_2) \qquad (4)$$

The values of T_1, T_2, (A_1/L_0) and (A_2/L_0) were determined for each light curve by nonlinear least squares fitting of this equation beginning a few days after peak brightness to assure that only the decay portion contributed to the fits. The method used was a damped Gauss–Newton iteration.

The results of the fits are given in Table 1. The standard deviations were estimated from the covariance matrix but should be regarded only as approximations (see ch. 7, ref. 7). The values were checked by repeating the fits using the separable parameter algorithm of Golub and Pereyra[8].

For all light curves in the sample the fitted curves represented the data points well and gave low values for the sum of squares of residuals, but only if the data were very complete did the fits specify the parameters with high certainty. This is illustrated in Figs 1 and 2 which represent one of the best and one of the worst fits. In both cases the curves accurately represent the data, but for SN1962j, $\sigma(T_2)$ is very large relative to T_2. The condition that the s.d. of both 1/e lives be less than the parameter values themselves provided a criterion for rejecting incomplete light curves from the sample.

Figure 3 is a plot of T_2 against T_1 with the error bars representing 1 s.d. The vertical and horizontal dashed lines represent the upper limits imposed by the terrestrial values. Only one point lies >1 s.d. beyond these limits, that point being ~ 2 s.d. out. Furthermore, there is a definite tendency for the points to lie along the predicted line $T_2 = 12.7\,T_1$ which is shown as a diagonal. Although the scatter is large, the correlation coefficient is $r = 0.529$, implying, at the 97.5% level of significance, that the data follow a non-random relationship. The average values of $\sigma(T_1)/T_1$ and $\sigma(T_2)/T_2$ are 0.13 and 0.43, a fact which invalidates both a standard regression of T_2 on T_1, which would

Fig. 2 Sum of exponentials fit to the light curve of SN1962j. Data points are taken from Bertola[12].

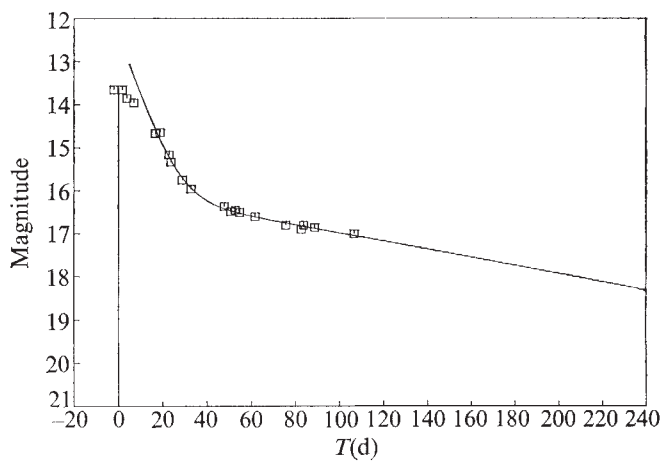

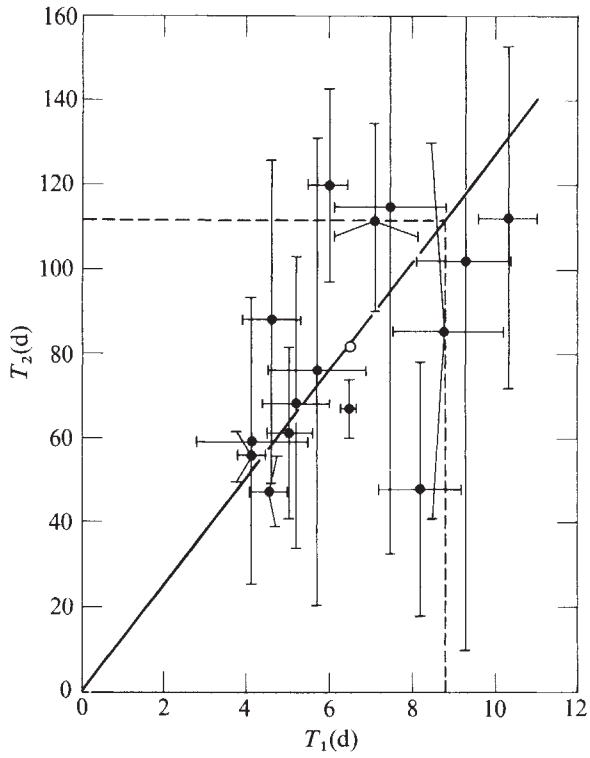

Fig. 3 Plot of the fitting parameters T_2 against T_1. The error bars represent the estimated s.d. but should not be interpreted as the major axes of error ellipsoids because the errors in T_1 and T_2 are correlated in each case.

assume the errors in T_1 are insignificant, and a major-axis regression, which would assume approximately equal errors in T_1 and T_2. It is, however, possible to use the computer generated T_1,T_2 variance matrices to obtain a maximum likelihood estimate of the best linear representation of the data (see ch. 4, ref. 7). The likelihood function can also be used to construct confidence regions in the space of the two parameters, that is, slope and intercept (ch. 7, ref. 7). When this procedure was applied to the data the point defined by equation (2), that is, slope = 12.7, intercept = 0, was found to lie well inside the 50% contour. This shows that the data are consistent with the predicted relation. A more dramatic measure of this consistency is furnished by the average values of T_1 and T_2 which are

$$\overline{T_1} = 6.46 \pm 1.98$$
$$\overline{T_2} = 81.2 \pm 25.7$$

where the indicated errors are the s.d. The point represented by these values is shown in Fig. 3 as an open circle lying almost exactly on the predicted line. These results constitute significant evidence supporting the $^{56}Ni \rightarrow {}^{56}Co \rightarrow {}^{56}Fe$ decay hypothesis. Furthermore, if the cold white dwarf model is correct, the fact that no T_2 is < 47 d implies an upper mass limit of $\sim 0.4 M_\odot$ for white dwarfs produced.

The authors would like to thank Ms Barbara J. Handley for assistance with the statistics and Professor Gene H. Golub for his nonlinear least squares program.

BERT W. RUST

Computer Sciences Division,
Oak Ridge National Laboratory,
Union Carbide Corporation, Nuclear Division,
Oak Ridge, Tennessee 37830

M. LEVENTHAL
S. L. MCCALL

Bell Laboratories,
Murray Hill, New Jersey 07974

Received November 24, 1975; accepted May 12, 1976.

1 Van Hise, J. R., *Astrophys. J.*, **192**, 657–659 (1974).
2 Colgate, S. A., and McKee, C., *Astrophys. J.*, **157**, 623–643 (1969).
3 Leventhal, M., and McCall, S. L., *Nature*, **255**, 690–692 (1975).
4 Rust, B. W., thesis, Univ. Illinois (1974).
5 Pskovskii, Yu. P., *Soviet Astr.* **11**, 570–575 (1968).
6 Pskovskii, Yu. P., *Soviet Astr.*, **14**, 798–805 (1971).
7 Bard, Y., *Nonlinear Parameter Estimation* (Academic, New York, 1974).
8 Golub, G. H., and Pereyra, V., *SIAM J. numer. Anal.*, **10**, 413–432 (1973).
9 Baade, W., and Zwicky, F., *Astrophys. J.*, **88**, 411–421 (1938).
10 Parenago, P., *Peremennye zvezdy*, **7**, 109–123 (1949).
11 Deutsch, A., *Poulkovo Observatory Circ.*, No. 28, 73–75 (1939).
12 Bertola, F., *Mem. Della Soc. Astr. Ital.*, **36**, 299–307 (1965).

Orientation of pulsar magnetic dipole moments

THE angle between the magnetic dipole moment and the spin of a pulsar is an important parameter in studies of the pulse emission. In this letter, arguments based on the properties of the weak interaction between elementary particles and on the superfluidity of the core show that the torque associated with the rotating dipole moment is free to cause alignment with the spin only in pulsars older than the Crab, and possibly the Vela pulsar. On the basis that the sine of the angle follows an exponential law with a time constant of $\sim 10^6$ yr, the observed distribution of radio pulse widths can be explained by the group of models in which emission occurs from regions near the polar caps rather than the light cylinder.

The high electrical conductivity[1] of the interior matter implies that the magnetic field of a pulsar should be fixed with respect to the body axes of the star. The principal moments, and the torque acting on the star, determine the orientation, as a function of time, of the magnetic dipole moment relative to the spin. The torque can be expressed as the sum of three components

$$\mathbf{N} = \mathbf{N}_1 + \mathbf{N}_2 + \mathbf{N}_3$$

where $\mathbf{N}_1$ and $\mathbf{N}_2$ represent the electromagnetic torque and are, respectively, perpendicular and parallel to the magnetic dipole moment $\mathbf{p}$. The component $\mathbf{N}_1$ can be approximated by the vacuum torque for the rotating external dipole field, and $\mathbf{N}_2$ represents the torque resulting from current flow between the corotating magnetosphere and the polar caps of the star. The component $\mathbf{N}_3$ represents the dissipative torque, which causes the axis of greatest principal moment to align with the spin. Owing to the temperature- and therefore time-dependence of $\mathbf{N}_3$, the angle ψ between spin and dipole moment is predicted for pulsars with the properties: (1) a mass such that there is no solid core; (2) an internal toroidal magnetic field with symmetry axis approximately colinear with $\mathbf{p}$, to have the following time variation. At a time $t_1 \lesssim 10^3$ yr, ψ becomes approximately equal to $\pi/2$ and remains constant until $t_2 \gtrsim 10^4$ yr. For $t > t_2$, $\psi \rightarrow 0$ with a time constant determined by $\mathbf{N}_1$, $\mathbf{N}_2$ and by the values of ψ and of the period P at $t = t_2$. This form of $\psi(t)$ is consistent with the existence of a strong interpulse in the Crab pulsar and, if the slowing of the pulsar rotation is determined mainly by $\mathbf{N}_1$, provides a simple explanation of the secular variation of magnetic dipole moment postulated by Lyne, Ritchings and Smith[2].

This prediction of $\psi(t)$ depends only on general features of superfluidity and of the non-leptonic weak interaction. Accurate knowledge of energy gaps or of the equation of state is not required.

At certain radii in the interior, neutrons, protons and Σ^- hyperons are expected to be in equilibrium. The protons[3] form an isotropic BCS superfluid with energy gap Δ. For such densities, the neutrons[4] may have a small anisotropic energy gap. If the proton energy gap alone is considered, the relaxation time for the non-leptonic weak interaction $n+n \leftrightharpoons p+\Sigma^-$ is proportional[5] to $(\beta\Delta)^{-5/2} \exp(\beta\Delta)$ in the limit $\beta\Delta \gg 1$, where $\beta^{-1} = k_B T$. If the spin is not parallel with the axis of greatest principal moment, the matter in the interior is subject to periodic pressure fluctuations having the period of the precession which must occur. As the pulsar cools, the relaxation time must increase until of the order of the precession period so